




Excited-State N Atoms Transform Aromatic Hydrocarbons into N-Heterocycles in Low-Temperature Plasmas

Journal Article

Author(s):

[Begley, Alina](#) ; [Shuman, Nicholas S.](#); [Long, Bryan A.](#); [Kämpf, Robin](#) ; [Gyr, Luzia](#); [Viggiano, Albert A.](#); [Zenobi, Renato](#) 

Publication date:

2022-03-17

Permanent link:

<https://doi.org/10.3929/ethz-b-000539166>

Rights / license:

[In Copyright - Non-Commercial Use Permitted](#)

Originally published in:

The Journal of Physical Chemistry A 126(10), <https://doi.org/10.1021/acs.jpca.1c10657>

Excited State N-Atoms Transform Aromatic Hydrocarbons into N-Heterocycles in Low-Temperature Plasma

Begley, Alina I.¹; Shuman, Nicholas S.²; Long, Bryan A.³; Kämpf, Robin¹; Gyr, Luzia⁴; Viggiano, Albert A.²; Zenobi, Renato*¹

¹Departement Chemie und Angewandte Biowissenschaften, ETH Zürich, 8093 Zürich, Switzerland, zenobi@org.chem.ethz.ch

²Air Force Research Laboratory, Space Vehicles Directorate, Kirtland AFB, New Mexico 87117, USA, rvborgmailbox@us.af.mil

³NRC postdoc at Air Force Research Laboratory, Space Vehicles Directorate, Kirtland Air Force Base, New Mexico 87117

⁴Leibniz Institute for Natural Product Research and Infection Biology – Hans Knöll Institute, Adolf-Reichwein-Straße 23, 07745 Jena, Germany

1. Abstract

The direct formation of *N*-heterocycles from aromatic hydrocarbons has been observed in nitrogen-based low-temperature plasma; the mechanism of this unusual nitrogen-fixation reaction is the topic of this paper. We used homologous aromatic compounds to study their reaction with reactive nitrogen species (RNS) in a dielectric barrier discharge ionization source (DBDI). Toluene (C₇H₈) served as a model compound to study the reaction in detail, which leads to the formation of two major products at “high” plasma voltage: a nitrogen replacement product yielding protonated methylpyridine (C₆H₈N⁺) and a protonated nitrogen addition (C₇H₈N⁺) product. We complemented those studies by a series of experiments probing the potential mechanism. Using a series of selected-ion flow tube (SIFT) experiments, we found that N⁺, N₂⁺, N₄⁺ react with toluene to form a small abundance of the *N*-addition product, while N(⁴S) reacted with toluene cations to form a fragment ion. We created a model for the RNS in the

plasma using variable electron and neutral density attachment mass spectrometry (VENDAMS) in a flowing afterglow Langmuir probe (FALP) apparatus. These experiments suggested that excited state nitrogen atoms could be responsible for the *N*-replacement product. Density functional theory (DFT) calculations confirmed that the reaction of excited state nitrogen $N(^2P)$ and $N(^2D)$ with toluene ions can directly form protonated methylpyridine, ejecting a carbon atom from the aromatic ring. $N(^2P)$ is responsible for this reaction in our DBDI source, as it has a sufficient lifetime in the plasma and was detected by optical emission spectroscopy (OES) measurements, showing an increasing intensity of $N(^2P)$ with increasing voltage.

2. Introduction

Nitrogen heterocycles (*N*-heterocycles) are the chemical building blocks for life as we know it, from the nucleobases in DNA to amino acids that form peptides and proteins. Understanding chemical pathways for the formation of *N*-heterocycles can give insights into their origin in primordial earth and extraterrestrial environments. A new pathway for the formation of *N*-heterocycles has recently been reported in a nitrogen-based low temperature plasma by the direct substitution of a carbon with a nitrogen in aromatic hydrocarbons.^{1,2} However, the mechanism by which a stable aromatic ring may be broken and a carbon atom replaced with a nitrogen atom from elemental N_2 has been unclear, because the reactive species in low-temperature plasmas are only partly characterized and the reaction mechanisms are not fully understood.³⁻⁶

Plasmas are ionized gases and considered the fourth state of matter; they are highly energetic, reactive and responsive to electric and magnetic fields. The properties of plasmas can be tuned widely depending on the degree of ionization, the type of gas being ionized, and whether the energy of the electrons is in equilibrium with the ions inside the plasma. Low-temperature plasmas, sometimes referred to as non-thermal

plasmas, are non-equilibrium plasmas in which the energy of the electrons is high (here we estimate 8-16 eV), but the ions and neutrals remain near room temperature.^{7,8} In the low-temperature plasma source used here, this type of non-equilibrium plasma is achieved using a dielectric barrier discharge ionization source (DBDI), in which high voltage alternating current is applied between two electrodes separated by a glass dielectric. Using nitrogen as the plasma gas, this leads to filamentary discharges and the formation of reactive nitrogen species (RNS).

Experiments with low-temperature plasmas have been used to mimic reactive species found in extraterrestrial environments, such as N^* , N^+ , N_2^+ to gain insights into astrochemistry.⁹ For example in the famous Urey-Miller experiment, electric discharges were passed through a “primordial gas mixture” of methane, nitrogen, and ammonia, which led to biologically relevant molecules including *N*-heterocycles.^{10,11} A significant portion of the atmospheres of Jupiter and Titan - a moon of Saturn - are nitrogen and methane, with a layer of aromatic hydrocarbons, including benzenes.¹²⁻¹⁴ Polyaromatic nitrogen heterocycles (PANHs) have been postulated in to be present Titan’s atmosphere, and *N*-heterocycles have been detected in carbaceous chondrites.^{15,16} Suggested pathways for the formation of *N*-heterocycles in extraterrestrial environments include UV irradiation of polycyclic aromatic hydrocarbons (PAHs) in ices to form alcohols, quinones, and ethers.¹⁷ The chemical pathways to explain the abiotic incorporation of nitrogen into complex hydrocarbons still remain to be explored.

While the direct replacement of a carbon with a nitrogen in the ring of aromatic hydrocarbons has been observed in low temperature plasmas, it is unclear how this reaction is possible. Ouyang *et al.* suggested that a reactive H_2ONO^+ species is formed in the low temperature plasma, which leads to type of aromatic substitution followed by ring opening and closing, with further investigation recommended.¹ Recent reports

suggest that excited state nitrogen, $N(^2D)$, may react with benzene and toluene to form pyridine and methylpyridine, respectively,¹⁸⁻²¹ and is supported by earlier reports of that reactions of active nitrogen with benzene lead to small yields of isocyanide, benzonitrile, and pyridine.^{22,23}

In this paper, we use a low temperature plasma generated with a cylindrical DBDI operated with a nitrogen atmosphere at atmospheric pressure.^{8,24,25} It is directly coupled to a high resolution mass spectrometer to monitor the reaction products. We demonstrate that, at elevated operating voltages, aromatic hydrocarbons are directly converted to *N*-heterocycles in a nitrogen-replacement reaction. We also observe a nitrogen-addition reaction and the formation of dimer species containing N. We disprove the hypothesis that NO^+ or H_2ONO^+ react with neutral species to form the *N*-replacement product by observing the products of substituted aromatic hydrocarbons. We confirm that the *N*-replacement reaction only takes place for aromatic hydrocarbons and that it is an aromatic carbon that is replaced with a nitrogen, by observing the reaction products of deuterated analogues and comparing the ionization products of reference compounds.

We found that the *N*-addition product was the result of N_2^+ and N_4^+ reacting with neutral toluene by reacting nitrogen ions N_x^+ ($x=1...4$) with toluene in a selected ion flow tube (SIFT). Furthermore, ground state N atoms $N(^4S)$ were found to react with toluene ions in the SIFT to form a fragmentation product. We finally conclude that the *N*-replacement product is formed by excited state N atoms $N(^2P)$ reacting with toluene radical cations after carrying out experiments using the flowing afterglow Langmuir probe method dubbed variable electron and neutral density attachment mass spectrometry (VENDAMS). These experiments allowed us to create a model of all reactions taking place in the plasma. DFT calculations supported our hypothesis that $N(^2P)$ leads to the *N*-replacement product. We finally confirmed the presence and

voltage dependent of an increase of $N(^2P)$ density inside our plasma using optical emission spectroscopy.

3. Materials and Methods

We have used a variety of complementary methods to understand how N atoms can enter an aromatic ring. Figure 1 shows schematics of all the methods, the question(s) addressed by that experiment, and what actually was studied.

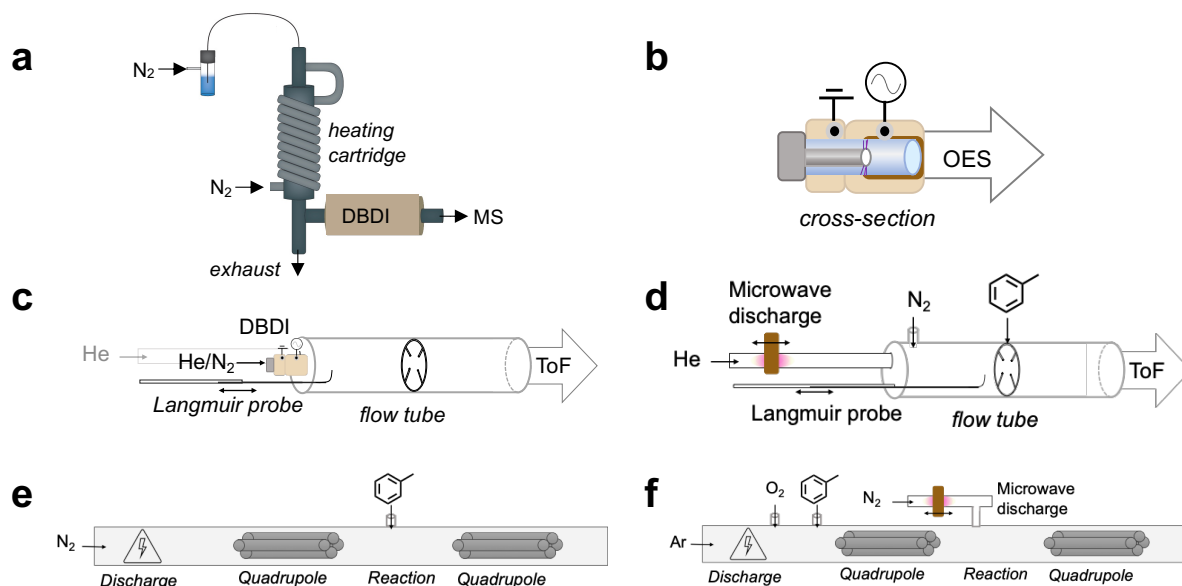


Figure 1: Overview of experimental methods, setup, and questions addressed: a) *DBDI-Orbitrap-MS* was used to investigate the products of aromatic hydrocarbons in nitrogen-based low-temperature plasma; b) *Optical emission spectroscopy* was used to identify excited state $N(^2P)$ atoms in the DBDI at atmospheric pressure, which increased with increasing operating voltage. c) In *DBDI-FALP-ToF-MS* the DBDI source was attached to the flow tube apparatus to investigate the charged reactive nitrogen species formed and compare the electron density at varying voltage using a Langmuir probe; d) *VENDAMS using FALP-ToF-MS* the RNS alone and toluene products were measured by varying electron density to build a model of the reactions leading to the N-addition and replacement products; e) *Selected ion flow tube (SIFT-MS)* was used to identify the products and rate constants of individual ion-molecule reactions $N_x^+(x=1\dots4) + C_7H_8^+$; f) a *modified SIFT-MS* was used for the ion molecule reaction $N(^4S) + C_7H_8$.

3.1. Dielectric Barrier Discharge Mass Spectrometry (DBDI-Orbitrap-MS)

The DBDI source, operated in an active capillary configuration, has been described previously.²⁴ Briefly, it contains an inner electrode (ground, stainless steel, ID: 0.6 mm and OD: 1.0 mm) and an outer electrode (copper, ID: 1.55 mm) to which a sine-modulated high voltage (2.4-3.8 kV_{pp}, 47.8 kHz) is applied, separated by a glass capillary. The applied voltage was determined by an external oscilloscope. The DBDI

source was screwed onto a custom-made ion transfer tube (heated to 200°C), which led directly into the mass spectrometer (LTQ-Orbitrap, Thermo Fisher). Mass spectra were acquired with high resolution for higher masses ($\Delta m/m$ 30 000, Orbitrap, 50-250 m/z) and lower mass resolution for low masses (unit mass resolution, linear ion trap, 20-50 m/z). Parameters included: acquisition of a mass range of 50-250 m/z with 1 microscan and a maximum injection time of 500 ms (Orbitrap acquisition parameters defining how many ions are injected into the C-trap), a tube lens voltage of 45 V, a capillary voltage of 6 V, and a capillary temperature of 200 °C. CID spectra were acquired with both the linear ion trap and Orbitrap. After acquiring spectra of the N₂-DBDI in negative and positive mode, we found that the ion count in negative mode was negligible, indicating that negative charges were primarily electrons. Therefore, all spectra were recorded in positive ion mode. All DBDI measurements were measured in triplicate.

Gas phase analytes were dispersed in a heated plasma gas (N₂, 99.9995%) and passed through the DBDI source online into the mass spectrometer. Analytes were brought into the gas-phase via a liquid infusion system, which has been described in detail previously:²⁶ a pressurized sample vial (0.1-0.8 bar overpressure N₂) was connected through a fused silica-capillary (ID: 30 μm, OD: 100 μm, length: 63 cm) to a hollow heat cartridge (200°C, flushed with 3 L/min N₂ 99.9995 %). A constant flow rate of gas was ensured with a mass flow controller (Bronkhorst High Tech B.V., Ruurlo, The Netherlands). For blank measurements, only nitrogen flowed through the source. The blank or sample was introduced from the heat cartridge into the DBDI source and on to the mass spectrometer through the DBDI source at a rate of 1.24 L/min, which was determined by the pressure difference at the inlet of the mass spectrometer (55 mbar). The pressure difference was determined using a manometer

(PCE group, Southampton Hampshire, UK) at the capillary inlet of the mass spectrometer.

Benzene (99.7%), toluene (99%), ethylbenzene (99%), chlorobenzene (99.9%), hexafluorobenzene (99%), aniline (99%), benzonitrile (99%) were purchased from Sigma-Aldrich Chemie GmbH (Buchs, Switzerland). Mesitylene (>99%), 3-methylpyridine (>98%), and cyclohexane (99.5%) were purchased from Fluka (Steinheim, Germany). Benzene-d₆ 99.8% was purchased from Armar Chemicals (Döttingen, Switzerland). The gas phase concentration of the aromatic hydrocarbon was calculated in ppm_{mol} (mol analyte/mol gas) by calculating the mol of sample infused and dispersed in a constant flow rate of pure nitrogen plasma gas (see SI).

For optical emission spectroscopy measurements, a UV-vis spectrometer (Echelle Spectra Analyzer ESA 3000 EV, LLA Instruments GmbH, Berlin-Adlershof, Germany) was used. An optical fiber was used to measure the emission in the range of 200–850 nm. The measurements were carried out along the axis of the DBDI.

3.2. Dielectric Barrier Discharge Flowing Atmospheric Langmuir Probe (DBDI-FALP-ToF-MS)

The flowing atmospheric Langmuir probe (FALP) consists of a 1 m long, 7 cm diameter, stainless-steel flow tube with a microwave discharge cavity on a 2.5 cm diameter arm upstream. The flow tube apparatus is used to measure individual plasma reactions under controlled conditions, as explained in the next subsection. In a first step, we ensured that the nitrogen species generated in the FALP were appropriate to simulate the reactions observed in the DBDI source by connecting the DBDI source directly to the FALP (DBDI-FALP-ToF-MS). A helium nitrogen gas mixture (9:1 v/v) was flowed through the DBDI source into the flow tube (14 std cm³ min⁻¹ helium and 10-30 std cm³ min⁻¹ of nitrogen) and operated at 2.5-3.5 kV_{pp} near atmospheric pressure (320 Torr). Using only nitrogen for the DBDI was not possible because the ion signal was

too low. Additional helium was added to achieve 8700 std cm³ min⁻¹ total of helium at 2.0 Torr in the flow tube, to increase flow. In a separate measurement, the Langmuir probe was moved to immediately after the DBDI source to compare the electron density at “low” and “high” (2.44 and 3.44 kVpp) operating voltages.

3.3. Flowing Atmospheric Langmuir probe (FALP) and Variable Electron and Neutral Density Mass Spectrometry (VENDAMS)

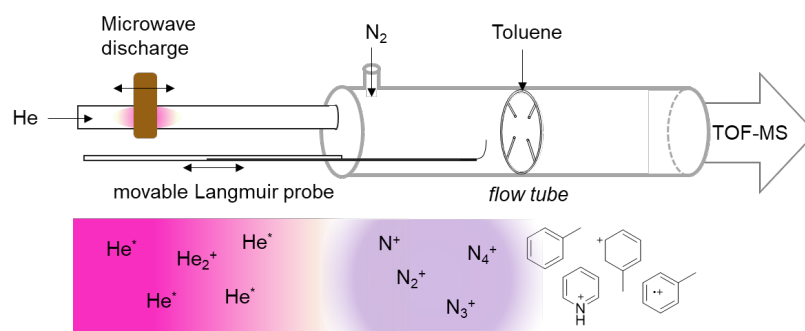


Figure 2: Schematic diagram of the AFRL flowing afterglow Langmuir probe (FALP), in which the helium is passed through a moveable microwave cavity to vary the electron density, which is measured using the Langmuir probe. A stream of nitrogen gas was introduced to generate reactive nitrogen species, which could, in turn, react with an analyte (toluene) added downstream. The ions were detected with a time-of-flight mass spectrometer.

Next, we carried out variable electron and neutral density attachment mass spectrometry (VENDAMS) measurements for the reaction of toluene with RNS (Figure 2). The measurements were carried out with the flowing afterglow Langmuir probe (FALP) at the Air Force Research Laboratory (AFRL) to help interpret the DBDI results, both the instrument and VENDAMS method have been described in detail previously.^{27,28} Helium (99.999%, Matheson, purified with a filter, Mono Torr) passes through a moveable microwave cavity to vary the plasma density. This produces a weakly ionized plasma consisting of He⁺, He₂⁺, He*, and e⁻, which is carried downstream into the flow tube. A flow of nitrogen (99.995%, Matheson) is added 10-50 cm downstream, converting the He⁺, He₂⁺, and He* to N⁺, N₂⁺, N₃⁺, N₄⁺, and possibly excited states of N₂* and N*. All flows were metered using mass flow controllers (MKS Instruments), with typical flows of 11.2 std. L min⁻¹ total of helium and 10 std. cm³ min⁻¹

of nitrogen. Measurements were carried out at room temperature at 1.0 Torr. Because the VENDAMS measurements with N₂ form multiple RNS, a complete set of data for the formation of the RNS with variable electron density was taken and analyzed according to the scheme shown in SI. That RNS-only dataset was then later used to help model the reactions with toluene. Acceptable agreement was found between the model and data. No negative ions were detected when the mass spectrometer was switched to negative polarity; thus, the positive charge was equal to the electron density and no negative ions were included in the model. Time of flight (TOF) mass spectra were measured at 10 electron densities ranging from 1×10⁹ to 5×10¹⁰ cm⁻³. The procedure was repeated with toluene added 50 cm downstream of the nitrogen gas inlet at 5.5 std. cm³ min⁻¹, resulting in a toluene concentration of 9.5×10¹² cm⁻³, and a reaction time 7 ms. The electron density was measured using the Langmuir probe at the appropriate gas entrance.

For both sets of data, the relative intensities of each product were plotted as relative branching ratios as a function of measured plasma density. A model was generated that iteratively solved the coupled rate equations. VENDAMS modelling has been described in detail previously,²⁷ and considers numerous reactions and their respective rate constants (see SI) to fit the acquired data. The N₂-only results were used as the starting point for the data containing both N₂ and toluene.

3.4. Selected-ion Flow Tube Mass Spectrometry (SIFT-MS)

To obtain rate constants for the above model and test a variety of postulated reactions, a selected-ion flow tube (SIFT) instrument was used to investigate individual reactive nitrogen ions N_x⁺ (x=1...4) with toluene (C₇H₈), as well as N atoms with toluene radical cations C₇H₈⁺. The ion source was a chemically versatile flow tube where helium (99.999%, Matheson, purified with a filter, Mono Torr, ~11.0 std. L min⁻¹) was passed through an electron impact ion source (tungsten filament).²⁹ For the N_x⁺ (x=1...4)

experiments, 1.0-2.0 std. L min⁻¹ flow of nitrogen gas (99.995%, Matheson) was added after the filament. Various nitrogen ion species were mass-selected using a quadrupole mass filter and injected against a pressure gradient into the reaction flow tube using a Venturi inlet. After several ms to allow for thermalization, toluene vapor was added downstream and the kinetics were measured.³⁰ Ions were sampled through a nose cone and detected using a quadrupole mass spectrometer with counting multiplier. Rate constants were determined from the exponential decay of the primary ions as a function of concentration (at least 10 concentrations). Product branching ratios were determined by fitting the data by modeling the assumed kinetics. Each rate constant was measured five times and averaged.

The same SIFT setup was modified to study the reaction of N atoms with the radical cation of toluene, C₇H₈⁺. For this experiment, the flow tube nature of the source was exploited. Ar (99.999%, Matheson 11.5 std. L min⁻¹) replaced the helium, since He⁺ reacts with O₂ to form O⁺ as well as O₂⁺ making the chemistry more complex. In contrast, Ar⁺ was quantitatively converted to O₂⁺ by adding O₂ (99.999%, Matheson, 70 std. cm³ min⁻¹) midway into the flow tube.³¹ Further downstream, toluene was added to almost exclusively form the radical cation C₇H₈⁺.³²⁻³⁵ The chemistry was pure enough that the SIFT quadrupole could be run in total transmission mode to increase the signal. The N atoms were produced by flowing 200 std. cm³ min⁻¹ of nitrogen through a microwave discharge (30 W). Mass spectra were acquired with the discharge on and off, with and without adding toluene. The concentration of N atoms [N] was estimated at 4.25×10¹² cm⁻³ (~1% dissociation) from the reaction of O₂⁺ (toluene turned off in the source) with N atoms (discharge on/off) using the known rate constant, k=8.0×10¹¹ cm³ s⁻¹, and the reaction time t of 4.7 ms.³⁶ This N atom concentration was used to determine the kinetics of C₇H₈⁺.

3.5. Density Functional Calculations

The reaction of a nitrogen atom with a toluene cation was explored using density functional calculations at the B3LYP/6-311++G(d,p) level using Gaussian 16 quantum chemical software.³⁷ Stationary points along several reaction coordinates were identified. Minima and transition states were confirmed to have 0 or 1 imaginary frequency, respectively. Intrinsic reaction coordinate (IRC) calculations confirmed connectivity between transition states and minima. Open-shell species were evaluated for spin-contamination and wavefunction instability.

4. Results and Discussion

4.1. N-replacement and -addition Reactions in the Nitrogen DBDI

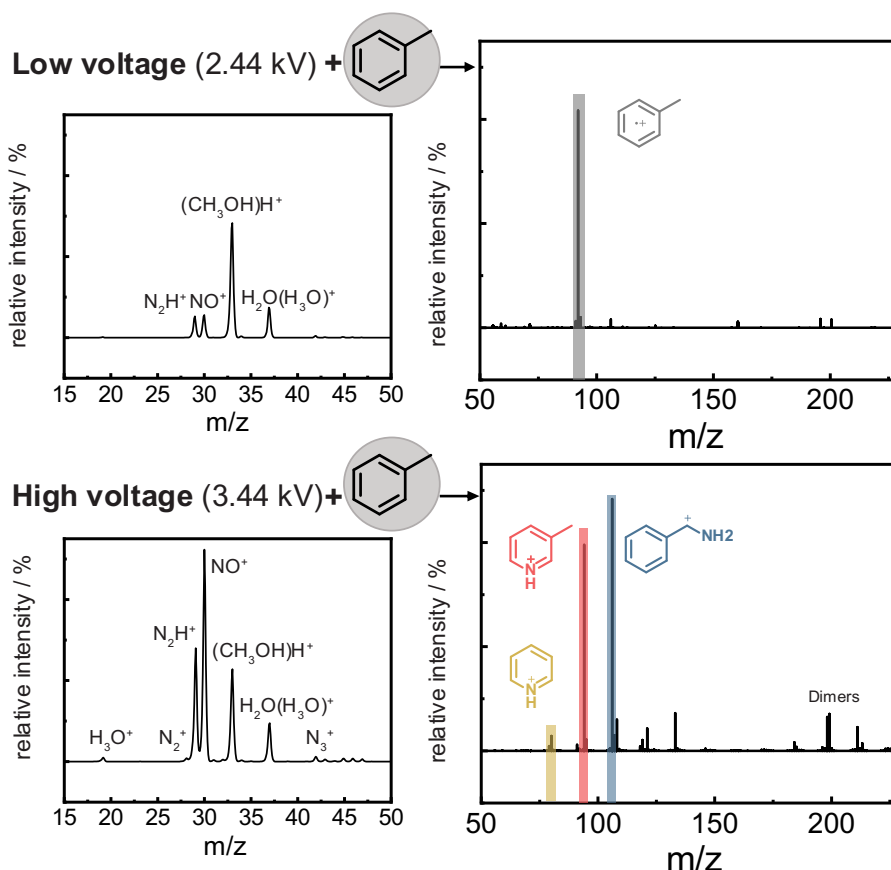


Figure 3: Type and abundance of reactive nitrogen species alone (*left*) in the DBDI shift from low (2.44 kV_{pp}) to high (3.44 kV_{pp}) voltage. When toluene is infused (5 ppm_{mol}, *right*), mainly the radical cation (C_7H_8^+) is formed at low voltages (2.44 kV_{pp}), but at high voltages (3.44 kV_{pp}) other plasma products are formed, including a N-replacement on the aromatic ring, a nitrogen addition (amination) product, and dimer species containing N. The ion intensities of the Orbitrap spectra (higher masses, *right*) and quadrupole data (lower masses, *left*) are displayed as relative intensities.

Typical mass spectra from the DBDI experiment are shown in Figure 3. The left spectra show the ionic reactive species generated in the plasma before the hydrocarbon is introduced. At low operating voltage (2.44 kV_{pp}), infusing toluene through the DBDI source results predominately in the intact radical molecular ion C₇H₈⁺ (Figure 3, top right, grey). However, at high voltage (3.44 kV_{pp}), we detect unusual product ions in large abundance: a nitrogen replacement in the aromatic hydrocarbon ring (Figure 3, bottom right, red) and a nitrogen addition (amination) product (Figure 3, bottom right, blue). We also observe low abundance dimer species containing N and pyridine (Figure 3, bottom right yellow). The product ions were assigned by using the exact mass provided by the high resolution Orbitrap mass spectrometer. We could therefore easily distinguish between the nitrogen-replacement product C₆H₈N⁺ and the H₂-addition product C₇H₁₀⁺ (not observed) by the mass difference (0.0132 m/z).

The nitrogen-replacement product is the result of an aromatic carbon atom being replaced by a nitrogen atom (C₆H₈N⁺), and was previously reported by Zhang *et al.* in a similar DBDI source in open atmosphere.¹ They likewise detected pyridine (C₅H₆N⁺), but not the N-addition product. They were able to collect the liquid product and confirm the replacement of a carbon with a nitrogen in the aromatic ring using GC-EI-MS experiments. However, because the reaction products were exposed to open atmosphere, they observed temporal variations and mixtures with oxygenated products, which we have been able to eliminate. While they observe co-production of [M+NOH₂]⁺ species and suggest that H₂ONO⁺ may be the reaction partner in an electrophilic aromatic substitution, we do not observe either ion, suggesting an alternative mechanism is responsible.

The most abundant product ion at high voltage is the N-addition product (C₇H₈N⁺), which likely corresponds to the amination product. There have not been any previous reports that this reaction occurs in aromatic hydrocarbons in low temperature plasmas.

However, product ions with a formal nitrogen addition $[M+N]^+$ have been previously reported for long aliphatic hydrocarbons (C_n , $n>40$) as an N-insertion resulting in iminium ions during paper-spray experiments,³⁸ or for shorter aliphatic hydrocarbons (C_n , $n=6-8$) in a 28-Torr N_2 hollow cathode with N_3^+ postulated as the source of N addition.³⁹ The presence of dimers containing an additional nitrogen as $[2M+N]^+$, $[2M-H+N]^+$ or $[2M-CH_2+N]^+$ are likely downstream products from these N-addition products. Such N-dimers form as a result of amination products, as previously reported by Usmanov *et al.*³⁹ and in experiments on benzyl- and alkylamines passed through a corona-discharge by Lee *et al.*⁴⁰

The nitrogen DBDI source generates a mixture of reactive nitrogen species (RNS) that interact with an infused sample and lead to production of intact molecular ions at low operating voltages. This includes charged species, like electrons and ions N_2^+ , N_3^+ , N_4^+ , and secondary product ions like NO^+ and N_2H^+ formed by reactions with minor impurities of water and oxygen. Nitrogen atoms $N(^4S)$ and electronically excited states N_2^* , $N(^2P)$, $N(^2D)$ and NO^* might also contribute to the ionization process.

We monitored the change in RNS with increasing voltage to elucidate which species are responsible for the N-replacement and -addition reactions at high voltages. As the voltage of the DBDI source is increased, NO^+ is the only low mass species (15-50 m/z) that increases significantly (see Figure S1a). However, previous optical emission spectroscopy measurements showed that as the voltage increased, the emission of N_2^+ also increased.⁸ Parallel to the increase in NO^+ , there was a decrease in the radical and protonated ions of toluene $C_7H_7^+$, $C_7H_8^+$, and $C_7H_9^+$ and an increase in the nitrogen addition and replacement products (see Figure S1b).

An increase in operating voltage in the DBDI source is related to an increase in electron density and energy, which leads to an increased number of filamentary microdischarges per unit of time.⁴¹ Peeters *et al.* report an increase in N atoms with

increasing voltage, and this is because the primary channel for the formation of atomic nitrogen in filamentary DBDIs is electron-impact dissociation of molecular nitrogen.^{42–}
⁴⁵ The increase of NO^+ with increasing voltage we observed is likely due to the reaction of excited state N atoms with trace impurities of oxygen atoms in the DBDI source. There are several production channels for NO^+ with RNS, but the reaction of $\text{N}(^2\text{P})$ with $\text{O}(^3\Sigma_g^-)$ is one of the faster reactions measured (see Table S2). We confirmed that $\text{N}(^2\text{P})$ was present in the DBDI source and rose with increasing operating voltage by optical emission spectroscopy (OES) (see Figure S2b). Confirming the presence of $\text{N}(^2\text{D})$ is not possible by OES, because the Einstein coefficient for the radiative transition to the ground state is too low.⁴⁶

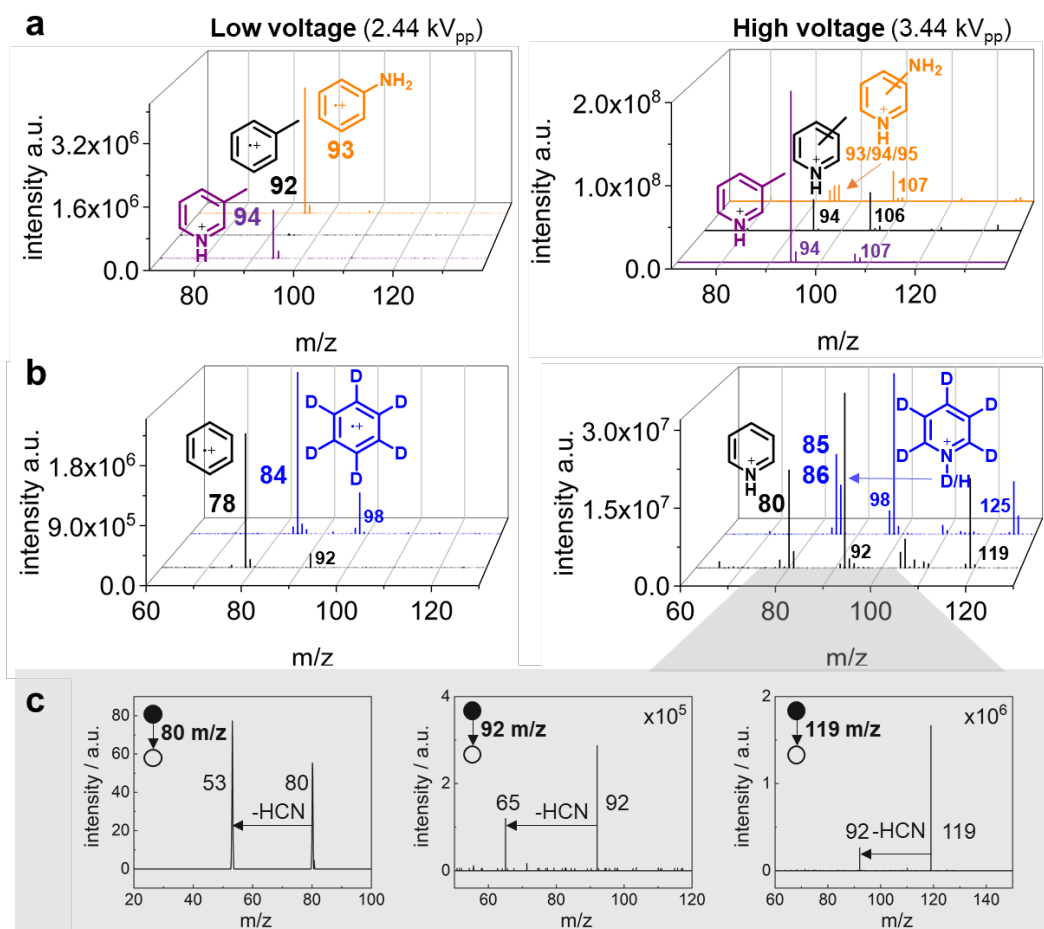


Figure 4: **a** Comparison of product ions detected of toluene (black) and reference compounds 3-methylpyridine (purple) and aniline (orange) at low (2.44 kV_{pp}) and high voltage (3.44 kV_{pp}). **b** Comparison of benzene (black) and deuterated benzene-d₆ (blue) at low (2.44 kV_{pp}) and high voltage (3.44 kV_{pp}). **c** CID experiments on major product ions detected from benzene at high voltage.

To confirm that the *N*-replacement product was the result of a nitrogen replacing a carbon inside the aromatic ring, we compared the ionization products of reference compounds, carried out CID experiments, and observed H/D exchange for the reaction with deuterated benzene. We confirmed that the detected *N*-replacement product ion of toluene at high voltages ($C_6H_8N^+$) was the result of a nitrogen replacement reaction in the ring by exposing isomeric reference compounds 3-methylpyridine (C_6H_7N) and aniline (C_6H_7N) to the same conditions. These compounds simulate the ionization of an *N*-replacement product in- and outside of the aromatic ring, respectively. We found that the product ions of 3-methylpyridine ($C_6H_8N^+$, 94 m/z, Figure 4b purple) correlate to those of toluene at high voltage, whereas the product ions of aniline form a mixture including the *N*-replacement product ($C_5H_7N_2^+$, 95 m/z, Figure 4b orange), the radical cation ($C_6H_7N^+$, 93 m/z), and protonated molecule ($C_6H_8N^+$, 94 m/z). The driving force for the formation of an *N*-heterocycle from an aromatic hydrocarbon may be its greater stability. While toluene tends to form radical cations at low voltages, methylpyridine has a high proton affinity and forms a protonated molecular ion.

Collision induced dissociation (CID) experiments confirmed that the *N*-replacement and -addition products of benzene are a *N*-heterocycle or an amine, respectively. The CID spectra of both of these products resulted in the loss of HCN, which can indicate an *N*-heterocycle or an amine (Figure 4c).

We also reproduced the nitrogen addition and replacement reactions for deuterated benzene. The observation of H/D-exchange, or lack thereof, can give information on the reaction mechanism leading to the products as well as on the acidity of the protons in the products formed. The protons originate from trace impurities in the nitrogen gas, as discussed previously. The *N*-addition product retained all deuterons, indicating that the addition of the nitrogen is outside of the ring. The *N*-replacement product leads to a mixture of one and no H/D exchanged. If the *N*-replacement product is formed via

electrophilic aromatic substitution as suggested by Zhang *et al.*, the abstraction of a deuteron from the ring is necessary for rearomatization (see Scheme S1).¹ However, we detected a mixture of $C_5D_6N^+$ and $C_5D_5HN^+$ from C_6D_6 , which contradicts this hypothesis (Figure 4b, blue). On the other hand, an *N*-replacement in the aromatic ring leads to the formation of an acidic N-D which is easily exchanged compared to an aromatic C-D. This could explain the observed mixture of $C_5D_6N^+$ and $C_5D_5HN^+$.

4.2. Reaction Scope

We investigated the scope of the reaction by varying the substituents on the aromatic ring. By varying the substituent between a hydrogen, methyl, or ethyl group, we detected similar major product ions and intensities. In each case, the most abundant product ion was the *N*-addition product $[M+N]^+$ (Figure 5, blue), followed by the *N*-replacement product $[M-C+N]^+$ (Figure 5, red). A minor product ion $[M+CN+NH]^+$ was detected for all three compounds (119, 133, 147 *m/z*, respectively), as well as a low abundance of dimer species containing N $[2M-H+2N]^+$ and $[2M+N]^+$ (see Table S3). The product ion corresponding to pyridinium ion $C_6H_5N^+$ (Figure 5, yellow) was detected for all compounds.

If the *N*-replacement reaction proceeded via an electrophilic aromatic substitution type reaction (see Scheme S1), in which the electron rich ring acts as a nucleophile and attacks a charged reactive nitrogen species, we would expect a higher relative intensity of the product formed if the aromatic ring is substituted with an electron donating group (EDG). Conversely, we expected a lower relative intensity if the aromatic ring has an electron withdrawing group (EWG), which deactivates the aromatic ring by withdrawing electron density. We chose chlorobenzene (C_6H_5Cl) as moderate EWG, benzonitrile (C_7H_5N) as a strong EWG, and aniline (C_6H_7N) as a strong EDG substituted aromatic compound to test this hypothesis and to avoid compounds that introduced oxygen into

the system. Surprisingly, we observed a decrease in the relative intensity of the *N*-replacement product for all substituted compounds, which contradicts the hypothesis that the reaction is initiated by an electrophilic aromatic substitution. Both aniline and benzonitrile at high voltage led to high abundances of protonated or radical cation (Figure 5, grey), rather than the *N*-replacement product.

If the nitrogen replacement reaction were to proceed by an addition of a nitrogen species onto the aromatic ring, we would expect that an *ortho* hydrogen needs to be available for rearomatization. To test this, we reacted 1,3,5-trimethylbenzene (mesitylene, C₉H₁₂), which effectively blocks every other position of the aromatic ring. Nevertheless, we observed the amination [M+N]⁺ and *N*-replacement products [M-C+N]⁺. To confirm that an aromatic C-H bond was necessary for the replacement product to form, we repeated the reaction with hexafluorobenzene, which blocks each aromatic position and is liquid at room temperature so that it can be easily introduced into the DBDI. A mixture of the radical cation (C₆F₆⁺, Figure 5, grey) and the nitrogen addition product (C₆F₆N⁺, Figure 5, grey) were formed. The formation of the nitrogen addition product indicates that an N atom likely binds as an adduct to the ring itself, not replacing an aromatic C-H bond. We also tested whether the nitrogen replacement reaction was specific to aromatic compounds or could be generalized for hydrocarbons by reacting cyclohexane (C₆H₁₂). We found that cyclohexane ionized as a deprotonated ion (C₁₂H₁₁⁺, Figure 5, grey) and also formed the amination product (C₁₂H₁₂N⁺, Figure 5, grey), but not the *N*-replacement product.

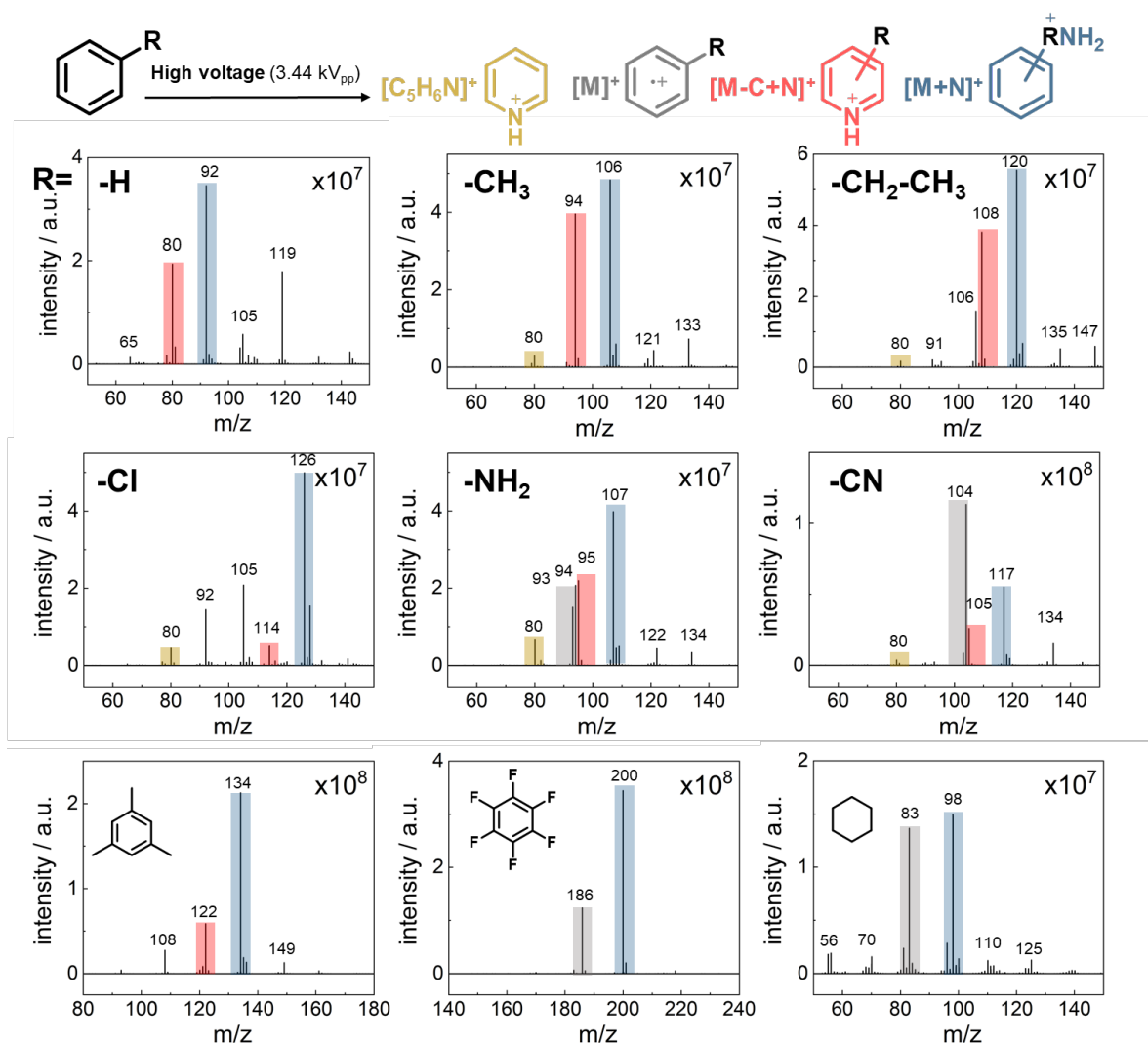


Figure 5: Product ions formed from (left to right, top to bottom) benzene, toluene, ethylbenzene, chlorobenzene, aniline, benzonitrile, mesitylene, hexafluorobenzene and cyclohexane at high voltage (3.44 kV_{pp}, each at approximately 5 ppm_{mol} gas phase concentration)

4.3. Mechanistic Investigation

To understand how a carbon atom in an aromatic ring can be directly replaced with a nitrogen atom after passing through the DBDI source, we studied the interaction of toluene with the RNS in controlled environments. With the VENDAMS method in the FALP, we were able to detect all of the products observed in the DBDI (Figure 6, right inset), albeit at much lower intensities. The most abundant products in the FALP were the radical cation (C₇H₈⁺, 92 m/z), and tropylium (C₇H₇⁺, 91 m/z) and the dimerization products.

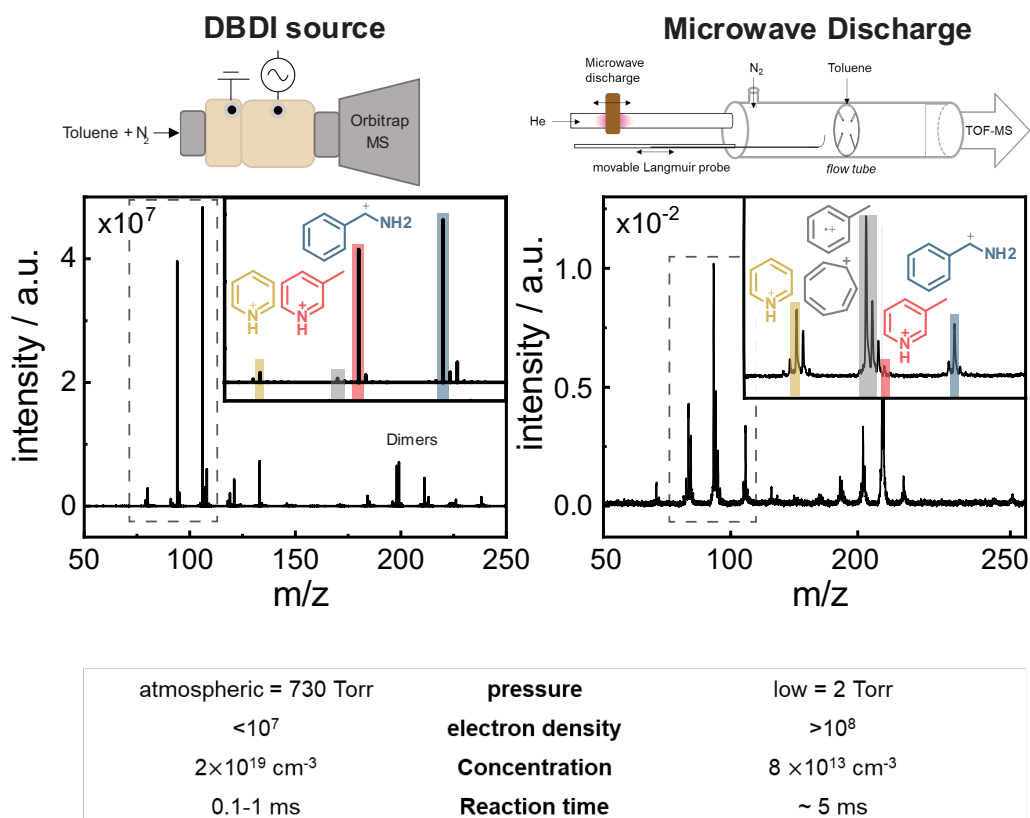


Figure 6: Comparison of the nitrogen-plasma products formed from toluene in the DBDI source and the microwave discharge of the FALP. The spectrum of the DBDI source is acquired on an LTQ-Orbitrap, while the FALP spectra are acquired with a TOF-MS.

We were able to increase the ratio of the nitrogen addition and replacement products relative to the molecular ions by increasing the pressure, and thereby concentration of toluene and reaction time, inside the flow tube (see Figure S3). However, after confirming that the RNS observed in the FALP could replicate those of the DBDI, we carried out measurements at low pressures (1 Torr), because this decreases impurities and generates more controllable reaction conditions that have been better characterized. The DBDI is operated at much higher pressure (760 Torr) than the FALP (1-5 Torr), resulting in significantly higher gas phase concentrations of toluene and presumably RNS. In the FALP setup, the RNS are formed by known dissociative recombination reactions and the reaction time can be precisely calculated.⁴⁷ The DBDI source contains an alternating high voltage electric field, resulting in complex behavior

that is difficult to model. Thus, the DBDI has a larger extent of reaction (concentration times time) but the FALP has more defined conditions.

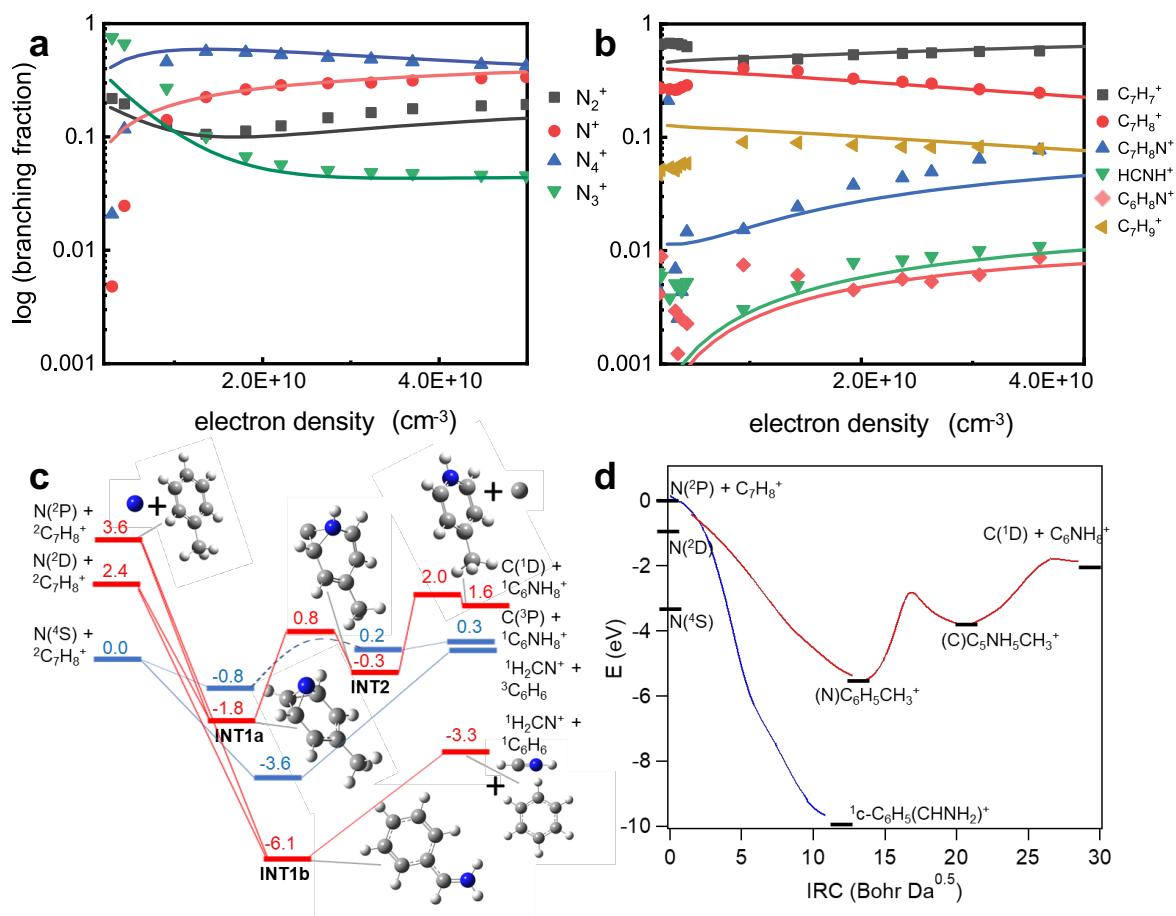


Figure 7: Relative fractions of the product ions detected as a function of varying electron density for **a)** the pure nitrogen plasma, and **b)** in the presence of toluene at 1 Torr. The points are fitted by iteratively solving the coupled rate equations of all expected reactions (see Table S4 and S5). The reactions hypothesized for different states of N atoms are tested by: **c)** calculated reaction coordinates of N + C₇H₈⁺ at the B3LYP/6-311++G(d,p) level along triplet (blue) and singlet (red) surfaces. Zero-point energy corrected energetics in eV are shown relative to N(⁴S) + ²C₇H₈⁺ reactants, where the leading superscript indicates multiplicity. Selected structures on the singlet surface are shown. The dashed curve on the triplet surface implies a transition state between the structures, but the stationary point was not identified. **d)** Intrinsic reaction coordinates calculated at the RB3LYP/6-311++G(d,p) level for N + C₇H₈⁺ on a singlet surface corresponding to initial attack of N toward the face of the toluene cation ring (red curve) or the methyl end of the toluene cation (blue curve). Electronic energies of calculated stationary points corresponding to INT1a, INT2 (red) and INT1b (blue) of c) are indicated.

We only considered ion-molecule reactions for the formation of N-addition and N-replacement products from toluene and RNS, as these have reactions kinetics which can lead to the products within the short reaction times in the DBDI (0.1-1 ms). Carrying out SIFT-MS experiments, we found that N⁺, N₂⁺, and N₄⁺ could react with neutral toluene at close-to-collisional rates to form small fractions of the N-addition product

(see Figure S4).⁴⁸ At high pressures in the DBDI, only N_2^+ and N_4^+ will contribute to this reaction pathway. This hypothesis is consistent with the increase in the N-addition product observed in the DBDI with increasing voltage, as the amount of N_2^+ increases as well.⁸ We found that the reaction with N_3^+ led exclusively to the radical cation.

Next, we hypothesized that ground state or excited state N atoms could be responsible for the N-replacement product. We were able to modify the SIFT-MS experiment to react ground state $N(^4S)$ atoms with toluene radical cations, which yielded mostly a fragment ion $C_6H_7^+$ at a rate constant of 2.3×10^{-11} (see Figure S5). Under the SIFT conditions, we were unable to generate a significant fraction of excited state N-atoms $N(^2D)$ or $N(^2P)$ to test their reaction with toluene ions.

Therefore, we used results from VENDAMS to model the RNS at varying electron densities, followed by using the same measurement and adding toluene. We generated a model by iteratively solving the coupled rate equations and fitting it to the experimental data. Using this model, we were able to fit the measured data reasonably well, albeit not perfectly. This indicates that most reactions and their rates were accounted for (Figure 7a, b) and predictions of concentrations of RNS can be made. After the N_2 -only plasma was well-modelled, we did the same for the experiment where toluene was added downstream. The reaction schemes are shown in Tables S4 and S5. The scheme without toluene addition shows that excited state N^* atoms are produced from dissociative recombination of N_3^+ with electrons.⁴⁷ The model showed that the excited state atoms could lead to the N-replacement product, such that performed density functional theory (DFT) calculations to confirm that this pathway is realistic. No dimerization products were included because of the complexity of the model – this is only as small perturbation and does not affect the modeling outside of error.

DFT calculations on the reactions of $C_7H_8^+$ with various states of N atoms support the experimental SIFT findings, indicating that ground state $N(^4S)$ atoms cannot form the N containing products directly on the singlet surface as they are spin-forbidden and energetically inaccessible. In contrast, both $N(^2P)$ and $N(^2D)$ can form the same entrance complex (INT1a) on a singlet surface in a barrierless processes, which ultimately results in the N-replacement product. In this intermediate, the nitrogen atom attacks a ring carbon, displaces the carbon from the plane of the ring, and results in a structure with the nitrogen and displaced carbon atoms approximately equidistant from the plane of the ring. Subsequently, the hydrogen atom may be transferred from the displaced carbon atom to the nitrogen atom over a barrier below the energy of reactants, yielding a product complex INT2, which may dissociate over a small reverse barrier yielding an excited state carbon atom and a protonated methyl pyridine cation. An analogous process may be possible on a triplet surface (spin-allowed for ground state $N(^4S)$), but the calculations failed to identify a key transition state and it then could not be confirmed that the reaction pathway exists. In any case the N-replacement product is endothermic (Figure 7c, blue).

Ground state $N(^4S)$ and toluene ions can react to yield, either a stabilized N-addition intermediate on the triplet surface (entrance complex INT1b), or a dissociation product from INT1b on the singlet surface resulting in $HCNH^+$ and benzene. The latter pathway supports the modified SIFT experiment of $N(^4S)$ reacting with toluene ions, which leads primarily to protonated benzene product ions.

Formation of either the N-addition or -replacement product from $C_7H_8^+$ with $N(^2D)$ or $N(^2P)$ on the singlet surface depends on the orientation of the toluene cation relative to the approach of the nitrogen atom (Figure 7d). If the nitrogen approaches the face of the ring, the intrinsic reaction coordinate follows attack and replacement of a ring carbon. If the nitrogen instead approaches the methyl group along the plane of the

ring, the N-addition pathway occurs in a barrierless fashion. The intrinsic reaction coordinates (IRC) (Figure 7d) show only the products of N(²P) and the toluene cation because they were performed using restricted DFT, which precludes description of the (²D) state; unrestricted calculations may show a similar, lower energy pathway for the (²D) state. We note that this same carbon-replacement pathway is accessible to other benzene derivatives where a hydrogen or hydrocarbon is initially bound to the replaced carbon, which is consistent with the observations described above in the DBDI source. Calculations of the N^{*} + C₆F₆⁺ system follow a similar pathway, but would terminate at the analogue of INT1a or INT2 in Figure 7c (i.e. the NC₆F₆⁺ adduct) as separated products C + C₅NF₆⁺ are calculated to be endothermic, even to reaction with N(²P). This is again consistent with the DBDI observations described above.

Dissociative recombination of N₂⁺ produces largely N(²D) along with a smaller quantity of N(²P),⁴⁷ as likely does dissociative recombination of either N₃⁺ or N₄⁺. Both excited states have sufficiently long radiative lifetimes to remain in the plasmas, ~ 10⁵ and 10 s, respectively,⁴⁹ but N(²D) has a shorter lifetime with respect to collisional quenching than does N(²P).⁵⁰ Under the flowing afterglow conditions, N(²D) has a half-life to collisional quenching of ~500 ms to He and ~60 ms to N₂, while the equivalent values for N(²P) are 5 s and 40 s, all longer than the time scale of the experiment.^{51,52} The collisional quenching rates of the excited nitrogen species with toluene are not known. Assuming those rate constants are similar to known values for other hydrocarbons, the half-life under the FALP conditions for N(²D) is ~1 – 4 ms (similar to the time scale of the experiment) and longer for N(²P) ~10 – 1000 ms.⁵² For the DBDI at atmospheric pressure, however, the half-life for N(²D) is 1 μs and for N(²P) is 0.9 ms. With a residency time of 0.3 ms in the DBDI source, only N(²P) has a sufficiently long lifetime to react.⁵²

While we were unable to generate enough electronically excited N atoms ($N(^2P)$ or $N(^2D)$) using a low-pressure microwave discharge for SIFT-MS experiments, the ratio of excited state to ground state atoms $N(^2P):N(^4S)$ increases from 1:100 to 1:1 when the pressure is increased from 20 Torr to 760 Torr.⁵³ Given that the DBDI at atmospheric-pressure shows a greater ratio of N-replacement product than the low-pressure flowing afterglow, it is likely that $N(^2P)$ reacts with toluene ions to form the N-replacement product in the DBDI. We also confirmed the presence and voltage dependent increase of this species using OES, as previously discussed.

Finally, the same calculated intermediates can also be accessed from charged RNS with neutral toluene. Calculations show that toluene can react with N_4^+ to eliminate an N_3 and access the singlet surface; in this case the N-replacement product is calculated to be endothermic, but the N-addition product is exothermic. This agrees with experimental SIFT-MS results, which showed that while mostly the radical cation was formed, a small branching fraction yielded the N-addition product (Figure S4). According to calculations, neutral toluene can react with ground state $N^+(^3P)$ to access the triplet surface or with N_3^+ to eliminate N_2 and access the singlet surface with large excess energy to yield the N-replacement products, respectively. However, the N-replacement product was not observed experimentally in SIFT-MS reactions of toluene with N^+ and N_3^+ .

5. Conclusions

In this work we demonstrate that aromatic hydrocarbons undergo N-addition and -replacement reactions to form *N*-heterocycles and amines, respectively. We identified the RNS responsible for each reaction in the nitrogen-based low temperature plasma. Through a process of elimination, we show that the nitrogen replacement reaction in aromatic hydrocarbons cations is likely due to excited state nitrogen atoms $N(^2P)$ or

$N(^2D)$. After characterizing all RNS in a controlled nitrogen microwave discharge plasma, we used SIFT-MS and flow tube experiments to exclude N_x^+ , ($x=1\dots4$) reacting with toluene molecules and $N(^4S)$ atoms reacting with toluene ions as being responsible for the *N*-replacement reaction. Observing that the *N*-replacement product increased with increasing voltage in the DBDI source alongside NO^+ and knowing that the density of excited N atoms increases with voltage and can react with O atoms from impurities to form NO^+ , we hypothesized that excited state N atoms were the reagent resulting in *N*-heterocycle formation. We used OES to confirm the presence of $N(^2P)$, which also rose with increasing DBDI voltage. Because of the challenges in generating and quantifying specific excited state N atoms, we iteratively solved the coupled rate equations of all RNS in the microwave discharge plasma. We were able to fit experimental data of toluene reacting with excited state N atom species with this model. We show that the reactions of $N(^2P)$ and $N(^2D)$ atoms with toluene ions $C_7H_8^+$ have pathways to products without energetic barriers above the reactant energy, but only $N(^2P)$ has a sufficient lifetime to react in the DBDI. The information resulting from these experiments serves as strong evidence that this is the responsible mechanism, despite no one individual experiment showing direct evidence independently.

Another major product observed after exposing the aromatic hydrocarbons to nitrogen-based low-temperature plasmas was the *N*-addition product, which is likely the formation of an amine but could also be a stable nitrogen adduct. Using flow tube experiments, we determined that N^+ , N_2^+ , N_4^+ can react with toluene to form the *N*-addition product. In the DBDI source, which operates at atmospheric pressure, only N_2^+ and N_4^+ will contribute to this reaction. Unlike the nitrogen replacement reaction, the nitrogen addition reaction is also observed in aliphatic hydrocarbons, specifically cyclohexane. We also observed nitrogen addition for an aromatic hydrocarbon with all carbons blocked by C-F bonds, in hexafluorobenzene C_6F_6 .

These insights into the role of excited state nitrogen in atmospheric, nitrogen-based low-temperature plasmas are important for understanding the chemistry of electric discharges and optimizing them for desired applications. Understanding the organic chemistry of excited state nitrogen atoms through low temperature plasmas for the formation of *N*-heterocycles offers alternate pathways for the extraterrestrial formation of life-sustaining chemistries.

6. Supporting Information

Details on calculation of gas phase concentration for DBDI-Orbitrap-MS; Values (dynamic viscosity, molecular weights, and densities) used for aromatic hydrocarbons; Overview of known reaction rate constants for the formation of NO⁺; Schematic of electrophilic aromatic substitution; Peak listings of aromatic hydrocarbons infused through DBDI source into Orbitrap-MS; Variation of branching fraction of RNS alone or toluene product ions with change in operating voltage; Optical emission spectra of DBDI source at low and high voltages; Reactions and rate constants used for modelling the RNS and toluene product ions in the FALP-TOF; Zero-point corrected energies of product channels in DFT calculations; Mass spectra of toluene product ions in FALP-TOF with varying pressure and flow conditions; Spectra of toluene products with selected ions N⁺, N₂⁺, N₃⁺, and N₄⁺, and their experimental rate constants; Schematic of modified SIFT and experimental rate constant for toluene radical cations with N(⁴S).

7. Acknowledgments

We thank the LOC mechanical workshop, especially Christian Marro, for designing and producing the DBDI source, and John Williamson for adapting the DBDI source to the flow tube experiments. Novartis is acknowledged for the donation of the LTQ-Orbitrap used in this study. We thank Cedric Wüthrich, Jonas Metternich, Irina Oganesyanyan and Mario Mirabelli for their helpful discussions. The AFRL authors acknowledge support

from the U.S. Air Force Office of Scientific Research under Grant AFOSR-19RVCOR042. B.A.L. was supported through the National Research Council–Research Associateship Program. The original data used in this publication are made available in a curated data archive at ETH Zurich (<https://www.researchcollection.ethz.ch>) under the DOI 10.3929/ethz-b-000519363. The mechanistic investigations at the Air Force Research Labs (AFRL) were made possible by USRA through the AFRL Scholars program and AFOSR- 19RVCOR042.

8. References

- (1) Zhang, Z.; Gong, X.; Zhang, S.; Yang, H.; Shi, Y.; Yang, C.; Zhang, X.; Xiong, X.; Fang, X.; Ouyang, Z. Observation of Replacement of Carbon in Benzene with Nitrogen in a Low-Temperature Plasma. *Sci. Rep.* **2013**, 3 (2), 6–10. <https://doi.org/10.1038/srep03481>.
- (2) Hosseini, H.; Saleem, M.; Marotta, E.; Paradisi, C. Nitrogen-Containing Organic Products from the Treatment of Liquid Toluene with Plasma-Activated N₂ Gas. *Plasma Process. Polym.* **2021**, 18 (5), 1–7. <https://doi.org/10.1002/ppap.202100012>.
- (3) Spedding, P. L. Chemical Synthesis by Gas-Phase Discharge. *Nature* **1967**, 214 (5084), 124–126. <https://doi.org/10.1038/214124a0>.
- (4) Suhr, H. Application of Nonequilibrium Plasmas in Organic Chemistry. *Plasma Chem. Plasma Process.* **1983**, 3 (1), 1–61.
- (5) Suhr, H. *Organic Synthesis under Plasma Conditions*; International Union of Pure and Applied Chemistry, 1974. <https://doi.org/10.1016/B978-0-408-70655-1.50008-9>.
- (6) Suhr, H. Organic Syntheses in the Plasma of Glow Discharges and Their Preparative Application. *Angew. Chem. Int. Ed.* **1972**, 11 (9), 781–792.

- (7) Fridman, A.; Fridman, A. Introduction to Theoretical and Applied Plasma Chemistry. *Plasma Chem.* **2009**, 1–11.
<https://doi.org/10.1017/cbo9780511546075.003>.
- (8) Gyr, L.; Klute, F.; Franzke, J.; Zenobi, R. Characterization of a Nitrogen-Based Dielectric Barrier Discharge Ionization Source for Mass Spectrometry Reveals Factors Important for Soft Ionization. *Anal. Chem.* **2019**, *91*.
<https://doi.org/10.1021/acs.analchem.9b01132>.
- (9) Dutuit, O.; Carrasco, N.; Thissen, R.; Vuitton, V.; Alcaraz, C.; Pernot, P.; Balucani, N.; Casavecchia, P.; Canosa, A.; Picard, S. Le; et al. Critical Review of N, N+, N₂, N⁺⁺, and N⁺⁺² Main Production Processes and Reactions of Relevance to Titan's Atmosphere. *Astrophys. Journal, Suppl. Ser.* **2013**, *204* (2). <https://doi.org/10.1088/0067-0049/204/2/20>.
- (10) Miller, S. L.; Urey, H. C. Organic Compound Synthesis on the Primitive Earth Published by : American Association for the Advancement of Science. *Science* (80-.). **1959**, *130* (3370), 245–251.
- (11) Johnson, A. P.; Cleaves, H. J.; Dworkin, J. P.; Glavin, D. P.; Lazcano, A.; Bada, J. L. The Miller Volcanic Spark Discharge Experiment. *Science* (80-.). **2008**, *322* (5900), 404. <https://doi.org/10.1126/science.1161527>.
- (12) Sagan, C.; Khare, B. N.; Thompson, W. R.; McDonald, G. D.; Wing, M. R.; Bada, J. L.; Vo-Dinh, T.; Arakawa, E. T. Polycyclic Aromatic Hydrocarbons in the Atmospheres of Titan and Jupiter. *Astrophys. J.* **1993**, *414*, 399–405.
- (13) Lebonnois, S. Benzene and Aerosol Production in Titan and Jupiter's Atmospheres: A Sensitivity Study. *Planet. Space Sci.* **2005**, *53* (5), 486–497.
<https://doi.org/10.1016/j.pss.2004.11.004>.
- (14) McCarthy, M. C.; Lee, K. L. K.; Loomis, R. A.; Burkhardt, A. M.; Shingledecker, C. N.; Charnley, S. B.; Cordiner, M. A.; Herbst, E.; Kalenskii, S.; Willis, E. R.; et

- al. Interstellar Detection of the Highly Polar Five-Membered Ring Cyanocyclopentadiene. *Nat. Astron.* **2021**, 5 (2), 176–180.
<https://doi.org/10.1038/s41550-020-01213-y>.
- (15) Peeters, Z.; Botta, O.; Charnley, S. B.; Ruiterkamp, R.; Ehrenfreund, P. The Astrobiology of Nucleobases. *Astrophys. J.* **2003**, 593 (2), L129–L132.
<https://doi.org/10.1086/378346>.
- (16) Peeters, E.; Hony, S.; Kerckhoven, C. Van; Tielens, A. G. G. M.; Allamandola, L. J. Astrophysics The Rich 6 to 9 μ m Spectrum of Interstellar PAHs. *Astronomy Astrophys.* **2002**, No. 390, 1089–1113.
- (17) Bernstein, M. P.; Sandford, S. A.; Allamandola, L. J.; Gillette, J. S.; Clemett, S. J.; Zare, R. N. UV Irradiation of Polycyclic Aromatic Hydrocarbons in Ices: Production of Alcohols, Quinones, and Ethers. *Science (80-.)*. **1999**, 283 (5405), 1135–1138. <https://doi.org/10.1126/science.283.5405.1135>.
- (18) Balucani, N.; Pacifici, L.; Skouteris, D.; Caracciolo, A.; Casavecchia, P.; Rosi, M. A Theoretical Investigation of the Reaction $N(2D) + C_6H_6$ and Implications for the Upper Atmosphere of Titan. In *Computational Science and Its Applications -- ICCSA 2018*; Gervasi, O., Murgante, B., Misra, S., Stankova, E., Torre, C. M., Rocha, A. M. A. C., Taniar, D., Apduhan, B. O., Tarantino, E., Ryu, Y., Eds.; Springer International Publishing: Cham, 2018; pp 763–772.
- (19) Balucani, N.; Pacifici, L.; Skouteris, D.; Caracciolo, A.; Casavecchia, P.; Falcinelli, S.; Rosi, M. A Computational Study of the Reaction $N(2D) + C_6H_6$ Leading to Pyridine and Phenylnitrene. In *Computational Science and Its Applications -- ICCSA 2019*; Misra, S., Gervasi, O., Murgante, B., Stankova, E., Korkhov, V., Torre, C., Rocha, A. M. A. C., Taniar, D., Apduhan, B. O., Tarantino, E., Eds.; Springer International Publishing: Cham, 2019; pp 316–324.

- (20) Rosi, M.; Falcinelli, S.; Casavecchia, P.; Balucani, N.; Recio, P.; Caracciolo, A.; Vanuzzo, G.; Skouteris, D.; Cavallotti, C. A Computational Study on the Attack of Nitrogen and Oxygen Atoms to Toluene. In *Computational Science and Its Applications -- ICCSA 2021*; Gervasi, O., Murgante, B., Misra, S., Garau, C., Blečić, I., Taniar, D., Apduhan, B. O., Rocha, A. M. A. C., Tarantino, E., Torre, C. M., Eds.; Springer International Publishing: Cham, 2021; pp 620–631.
- (21) Rosi, M.; Pacifici, L.; Skouteris, D.; Caracciolo, A.; Casavecchia, P.; Falcinelli, S.; Balucani, N. A Computational Study on the Insertion of N(2D) into a C---H or C---C Bond: The Reactions of N(2D) with Benzene and Toluene and Their Implications on the Chemistry of Titan. In *Computational Science and Its Applications -- ICCSA 2020*; Gervasi, O., Murgante, B., Misra, S., Garau, C., Blečić, I., Taniar, D., Apduhan, B. O., Rocha, A. M. A. C., Tarantino, E., Torre, C. M., et al., Eds.; Springer International Publishing: Cham, 2020; pp 744–755.
- (22) Brown, R.; Winkler, C. A. The Chemical Behavior of Active Nitrogen. *Angew. Chemie Int. Ed. English* **1970**, *9* (3), 181–196.
<https://doi.org/10.1002/anie.197001811>.
- (23) Dewurst, H. A. Chemical Reactions of Active Nitrogen. *J. Phys. Chem.* **1970**, *63* (3), 1976–1977.
- (24) Nudnova, M. M.; Zhu, L.; Zenobi, R. Active Capillary Plasma Source for Ambient Mass Spectrometry. *Rapid Commun. Mass Spectrom.* **2012**, *26* (12), 1447–1452. <https://doi.org/10.1002/rcm.6242>.
- (25) Gyr, L.; Wolf, J.-C.; Franzke, J.; Zenobi, R. Mechanistic Understanding Leads to Increased Ionization Efficiency and Selectivity in Dielectric Barrier Discharge Ionization Mass Spectrometry – A Case Study with Perfluorinated Compounds. *Anal. Chem.* **2018**, *90*. <https://doi.org/10.1021/acs.analchem.7b04711>.
- (26) Wolf, J. C.; Schaer, M.; Siegenthaler, P.; Zenobi, R. Direct Gas-Phase

- Detection of Nerve and Blister Warfare Agents Utilizing Active Capillary Plasma Ionization Mass Spectrometry. *Eur. J. Mass Spectrom.* **2015**, 21 (3), 305–312.
<https://doi.org/10.1255/ejms.1347>.
- (27) Shuman, N. S.; Miller, T. M.; Viggiano, A. A.; Troe, J. *Teaching an Old Dog New Tricks: Using the Flowing Afterglow to Measure Kinetics of Electron Attachment to Radicals, Ion-Ion Mutual Neutralization, and Electron Catalyzed Mutual Neutralization*; Elsevier Inc., 2012; Vol. 61.
<https://doi.org/10.1016/B978-0-12-396482-3.00005-3>.
- (28) Miller, T. M.; Miller, A. E. S.; Paulson, J. F.; Liu, X.; Miller, T. M.; Miller, A. E. S.; Paulson, J. F. Thermal Electron Attachment to SF₄ and SF₆. *J. Chem. Phys.* **2013**, 8841 (1994).
- (29) Van Doren, J. M.; Barlow, S. E.; Depuy, C. H.; Bierbaum, V. M. The Tandem Flowing Afterglow-Shift-Drift. *Int. J. Mass Spectrom. Ion Process.* **1987**, 81 (C), 85–100. [https://doi.org/10.1016/0168-1176\(87\)80007-1](https://doi.org/10.1016/0168-1176(87)80007-1).
- (30) Howard, C. J. Kinetic Measurements Using Flow Tubes. *J. Phys. Chem.* **1979**, 83 (1), 3–9. <https://doi.org/10.1021/j100464a001>.
- (31) Anicich, V. G. An Index of the Literature for Bimolecular Gas Phase Cation-Molecule Reaction Kinetics. *JPL-Publication-03-19* **2003**, No. November, 1194.
- (32) Williams, S.; Midey, A. J.; Arnold, S. T.; Morris, R. A.; Viggiano, A. A.; Chiu, Y. H.; Levandier, D. J.; Dressler, R. A.; Berman, M. R. Electronic, Rovibrational, and Translational Energy Effects in Ion-Alkylbenzene Charge-Transfer Reactions. *J. Phys. Chem. A* **2000**, 104 (45), 10336–10346.
<https://doi.org/10.1021/jp001428n>.
- (33) Melko, J. J.; Ard, S. G.; Shuman, N. S.; Viggiano, A. A. Temperature Dependences for the Reactions of Ar⁺, O²⁺, and C₇H₇⁺ with Toluene and Ethylbenzene. *Int. J. Mass Spectrom.* **2013**, 353, 60–66.

<https://doi.org/10.1016/j.ijms.2013.06.017>.

- (34) Arnold, S. T.; Dotan, I.; Williams, S.; Viggiano, A. A.; Morris, R. A. Selected Ion Flow Tube Studies of Air Plasma Cations Reacting with Alkylbenzenes. *J. Phys. Chem. A* **2000**, *104* (5), 928–934. <https://doi.org/10.1021/jp9928199>.
- (35) Fournier, J. A.; Shuman, N. S.; Melko, J. J.; Ard, S. G.; Viggiano, A. A. A Novel Technique for Measurement of Thermal Rate Constants and Temperature Dependences of Dissociative Recombination: CO₂⁺, CF₃⁺, N₂O⁺, C₇H₈⁺, C₇H₇⁺, C₆H₆⁺, C₆H₅⁺, C₅H₆⁺, C₄H₄⁺, and C₃H₃⁺. *J. Chem. Phys.* **2013**, *138* (15). <https://doi.org/10.1063/1.4801657>.
- (36) Martinez, O.; Sanchez, J. C.; Ard, S. G.; Li, A.; Melko, J. J.; Shuman, N. S.; Guo, H.; Viggiano, A. A. Selected-Ion Flow Tube Temperature-Dependent Measurements for the Reactions of O₂⁺ with N Atoms and N₂⁺ with O Atoms. *J. Chem. Phys.* **2015**, *142* (15), 1–7. <https://doi.org/10.1063/1.4916913>.
- (37) Frisch, M. J.; Trucks, G. W.; Schlegel, H. B.; Scuseria, G. E.; Robb, M. a.; Cheeseman, J. R.; Scalmani, G.; Barone, V.; Petersson, G. a.; Nakatsuji, H.; et al. Gaussian 16 Revision C.01. Gaussian, Inc.: Wallingford CT 2016.
- (38) Li, G.; Li, X.; Ouyang, Z.; Cooks, R. G. Carbon-Carbon Bond Activation in Saturated Hydrocarbons by Field-Assisted Nitrogen Fixation. *Angew. Chemie - Int. Ed.* **2013**, *52* (3), 1040–1043. <https://doi.org/10.1002/anie.201207997>.
- (39) Usmanov, D. T.; Chen, L. C.; Hiraoka, K.; Wada, H.; Nonami, H.; Yamabe, S. Nitrogen Incorporation in Saturated Aliphatic C₆–C₈ Hydrocarbons and Ethanol in Low-Pressure Nitrogen Plasma Generated by a Hollow Cathode Discharge Ion Source. *J. Mass Spectrom.* **2016**, No. March, 446–452. <https://doi.org/10.1002/jms.3765>.
- (40) Lee, S.; Kulyk, D. S.; Marano, N.; Badu-tawiah, A. K. Uncatalyzed N - Alkylation of Amines in Ionic Wind from Ambient Corona Discharge. *Anal.*

- Chem.* **2021**, 93, 2440–2448. <https://doi.org/10.1021/acs.analchem.0c04440>.
- (41) Gyr, L.; Wolf, J. C.; Franzke, J.; Zenobi, R. Mechanistic Understanding Leads to Increased Ionization Efficiency and Selectivity in Dielectric Barrier Discharge Ionization Mass Spectrometry: A Case Study with Perfluorinated Compounds. *Anal. Chem.* **2018**, 90 (4), 2725–2731. <https://doi.org/10.1021/acs.analchem.7b04711>.
- (42) Peeters, F. J. J.; Yang, R.; Van De Sanden, M. C. M. The Relation between the Production Efficiency of Nitrogen Atoms and the Electrical Characteristics of a Dielectric Barrier Discharge. *Plasma Sources Sci. Technol.* **2015**, 24 (4). <https://doi.org/10.1088/0963-0252/24/4/045006>.
- (43) Es-Sebbar, E. T.; Sarra-Bournet, C.; Naud, N.; Massines, F.; Gherardi, N. Absolute Nitrogen Atom Density Measurements by Two-Photon Laser-Induced Fluorescence Spectroscopy in Atmospheric Pressure Dielectric Barrier Discharges of Pure Nitrogen. *J. Appl. Phys.* **2009**, 106 (7). <https://doi.org/10.1063/1.3225569>.
- (44) Tsyganov, D.; Pancheshnyi, S. Simulation of N-Atom Production in Dielectric-Barrier Discharge in Nitrogen at Atmospheric Pressure. *Plasma Sources Sci. Technol.* **2012**, 21 (6). <https://doi.org/10.1088/0963-0252/21/6/065010>.
- (45) Popov, N. A. Dissociation of Nitrogen in a Pulse-Periodic Dielectric Barrier Discharge at Atmospheric Pressure. *Plasma Phys. Reports* **2013**, 39 (5), 420–424. <https://doi.org/10.1134/S1063780X13050085>.
- (46) Garstang, R. H. *The Air Glow and the Aurora*; Armstrong, B., E., Dalgarno, A., Eds.; Pergamon: London and New York, 1955.
- (47) Larsson, M.; Orel, A. E. *Dissociative Recombination of Molecular Ions*; Cambridge Molecular Science; Cambridge University Press, 2008. <https://doi.org/10.1017/CBO9780511535406>.

- (48) Su, T.; Chesnavich, W. J. Parametrization of the Ion–Polar Molecule Collision Rate Constant by Trajectory Calculations. *J. Chem. Phys.* **1982**, *76* (10), 5183–5185. <https://doi.org/10.1063/1.442828>.
- (49) Froese Fischer, C.; Tachiev, G.; Irimia, A. Relativistic Energy Levels, Lifetimes, and Transition Probabilities for the Sodium-like to Argon-like Sequences. *At. Data Nucl. Data Tables* **2006**, *92* (5), 607–812. <https://doi.org/https://doi.org/10.1016/j.adt.2006.03.001>.
- (50) Breckenridge, W. H.; Umemoto, H. Collisional Quenching of Electronically Excited Metal Atoms. *Dyn. Excit. State* **2007**, *50*, 325–393. <https://doi.org/10.1002/9780470142745.ch5>.
- (51) Sugawara, K.; Ishikawa, Y.; Sato, S. The Rate Constants of the Reactions of the Metastable Nitrogen Atoms, 2D and 2P, and the Reactions of N(4S)+NO->N2+O(3P) and O(3P)+NO+M->NO2+M. *Bulletin of the Chemical Society of Japan*. 1980, pp 3159–3164.
- (52) Herron, J. T. Evaluated Chemical Kinetics Data for Reactions of N(2D), N(2P), and N2(A3Σ+u) in the Gas Phase. *J. Phys. Chem. Ref. Data* **1999**, *28* (5), 1453–1483. <https://doi.org/10.1063/1.556043>.
- (53) Noxon, J. F. Active Nitrogen at High Pressure. *J. Chem. Phys.* **1961**, *36*, 926–940.

TOC Graphic

